## Supplement of

# Divergent iron dissolution pathways controlled by sulfuric and nitric acids from the ground-level to the upper mixing layer

Guochen Wang et al.

Correspondence to: Weijun Li (liweijun@zju.edu.cn)

### **Contents of this file**

Texts S1 and S2 Figures S1 to S10 Table S1 Reference

#### Texts S1. Atmospheric chemical transport model

Since size-resolved aerosol data were unavailable for Hangzhou, we simulated size-fractionated iron solubility using the Integrated Massively Parallel Atmospheric Chemical Transport (IMPACT) model (Ito and Miyakawa, 2023; Ito et al., 2019; Ito and Xu, 2014). The simulations were conducted at a horizontal resolution of  $2.0^{\circ} \times 2.5^{\circ}$  with 47 vertical layers, covering the observation period from September 11 to 21, 2021 (Hangzhou). The model was driven by MERRA-2 reanalysis meteorological data provided by NASA's Global Modeling and Assimilation Office (GMAO). IMPACT model simulates the emission, chemistry, transport, and deposition of aerosols and their precursors from anthropogenic, pyrogenic, lithogenic, oceanic, and biogenic sources. Iron solubility over Hangzhou was estimated for two aerosol size bins ( $D_p < 1 \mu m$  and  $D_p > 1 \mu m$ ).

As shown in Figure S5, while the model slightly overestimates Fe solubility compared to observations, the discrepancy remains within one order of magnitude ( $\pm 10$ ). The model also captures the elevated Fe solubility. The overestimation is likely due to a size mismatch: the model simulates Fe solubility for the  $D_p > 1~\mu m$  fraction, whereas the observations are based on total suspended particles (TSP), which include a broader particle size range.

#### Texts S2. Limited role of ligand-promoted pathway in Fe dissolution

Numerous studies have demonstrated that low-molecular-weight organic acids (e.g., oxalate) can form stable Fe-ligand complexes, thereby enhancing Fe solubility, particularly under mildly acidic conditions (pH > 3) (Sakata et al., 2022). Since direct measurements of organic acids were not available in our dataset, we were unable to explicitly quantify the contribution of ligand-promoted dissolution to the observed dissolved Fe. To provide a preliminary estimate of organic acid presence, we applied the empirical relationship proposed by Yu et al. (2005) to estimate oxalate from sulfate ([SO<sub>4</sub><sup>2-</sup>]):

$$[C_2O_4^{2-}] = 0.05 \times [SO_4^{2-}] - 0.273$$
 (E1)

where, [C<sub>2</sub>O<sub>4</sub><sup>2-</sup>] is oxalate concentrations in nmol m<sup>-3</sup>; [SO<sub>4</sub><sup>2-</sup>] is sulfate concentrations in nmol m<sup>-3</sup>.

Here, oxalate is used as a proxy due to its ubiquity and reactivity among atmospheric organic ligands (Ho et al., 2010; Fu et al., 2013). We estimated oxalate levels at the mountain site and Hangzhou and applied oxalate to total Fe molar ratio ([oxalate]/[FeT] as a proxy for ligand-promoted dissolution capacity (Shi et al., 2022; Zhang et al., 2022). As shown in Figure S10, no significant correlation was observed between Fe solubility (%Fes) and [oxalate]/[FeT] in the mountain and Hangzhou, suggesting that ligand-driven complexation played a minimal role in promoting Fe dissolution during the sampling period. The result indicates that proton-promoted mechanism was not the dominant pathway for aerosol Fe solubilization in our study.

While organic acids can contribute to iron solubilization, their concentrations are generally much lower than those of strong inorganic acids such as sulphuric and nitric acids. For example, Deshmukh et al. (2023) reported that oxalate-to-sulfate and oxalate-to-nitrate mass ratios of approximately 1:25 and 1:4, respectively, in fine particles ( $D_p < 1 \mu m$ ), and  $\sim 1:16$  and  $\sim 1:18$  in coarse particles ( $D_p > 1 \mu m$ ). In this study, oxalate concentrations in total suspended particles (TSP) were estimated following the approach described in the equation (E1), and the oxalate-to-(sulfate + nitrate) ratios were found to be 6% and 5% at the mountain and Hangzhou, respectively. At such low concentrations, we believe that the contribution of organic acids to iron dissolution is limited. What's more, our recent research (Li et al., 2025) also revealed that oxalate, like  $Ca^{2+}$ , was predominantly present in coarse-mode particles, peaking in the 3.2–5.6  $\mu$ m size bin—consistent with previous findings from Deshmukh et al. (2023). Since our study focused on TSP samples with larger particle size, the relative contribution of organic acids to Fe dissolution is expected to be low due to their relatively low loadings in the coarse fraction.

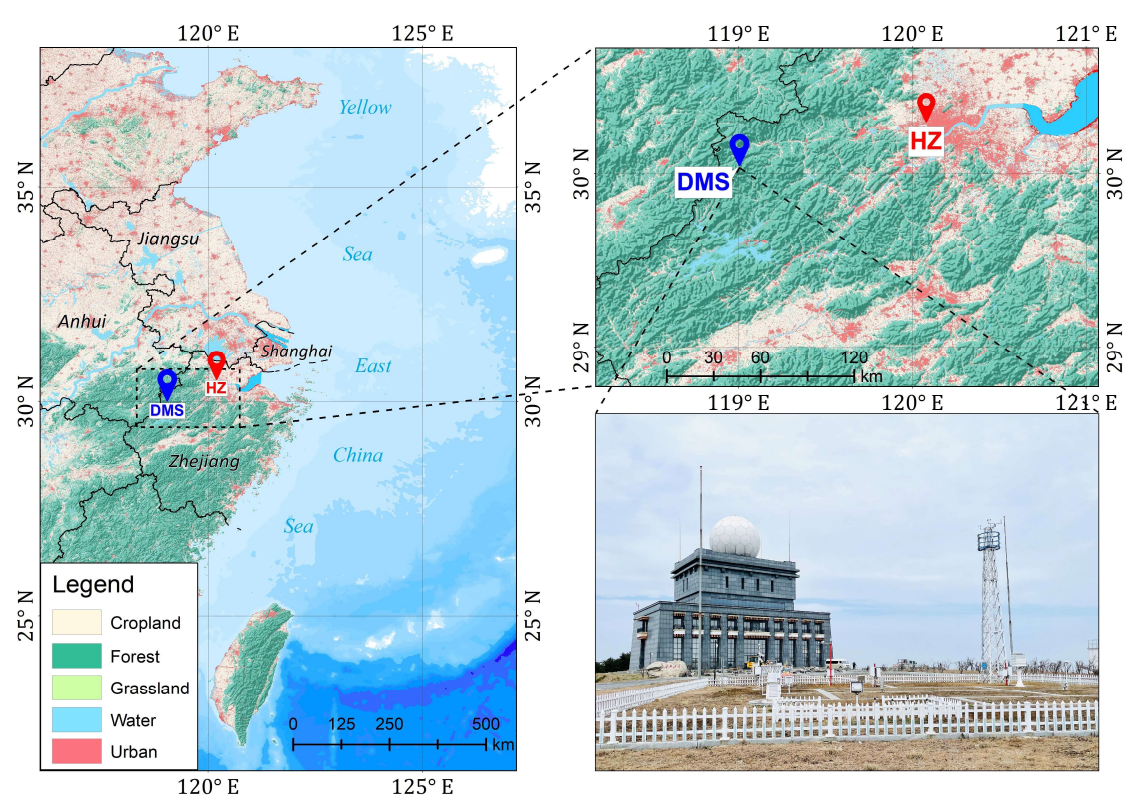


**Figure S1:** Map of the sampling sites. The symbols in the upper right panel denote the sampling sites located in the mountain site (DMS, 30.03° N, 119.00° E, 1483 m) and the megacity of Hangzhou (HZ, 30.30° N, 120.09° E, 6 m), respectively. Picture in the lower right panel was taken at the front of the mountain site. The background is the land use types of China in 2022 at a spatial resolution of 30 m (Yang and Huang, 2021). Map created by ArcGIS 10.3 (Esri, USA).

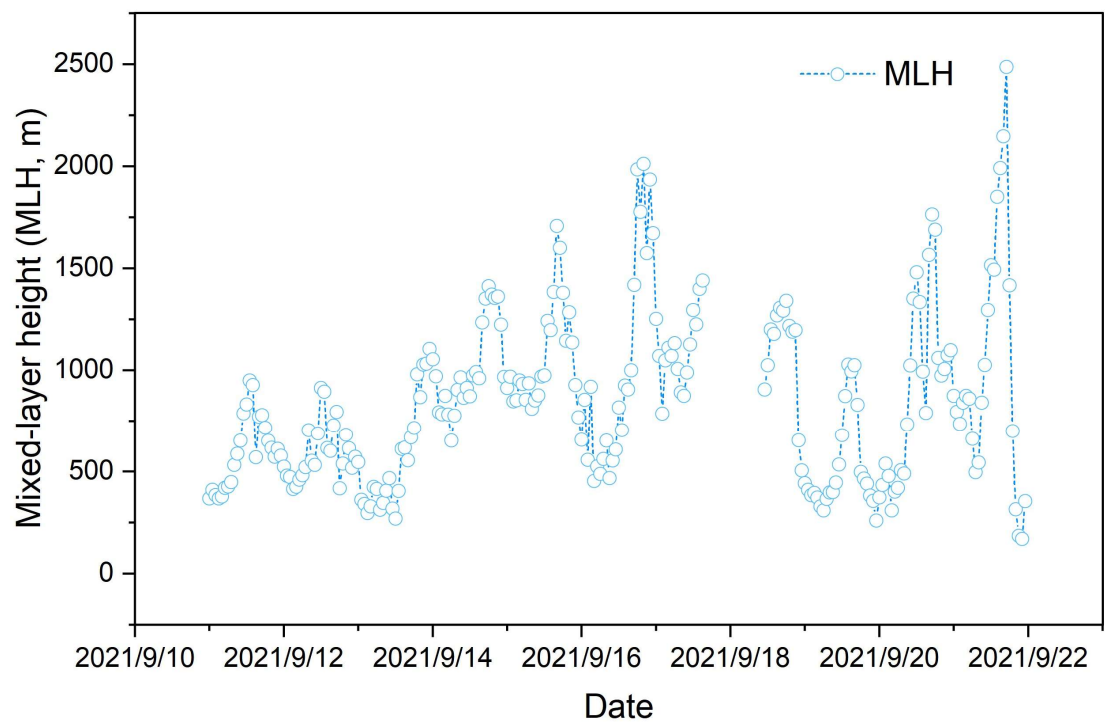


**Figure S2:** Time series of mixed-layer height (MLH) in Hangzhou during the sampling period (September 11 to 21, 2021).

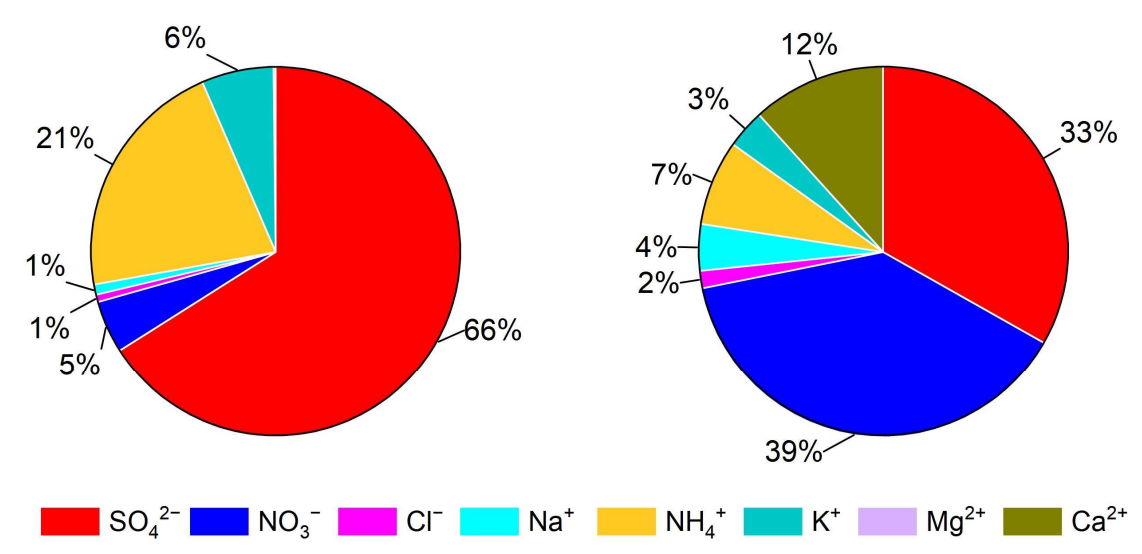


**Figure S3:** Percentage of the measured water-soluble inorganic ions in the sized-resolved aerosols collected in the upper mixing layer of the mountain (DMS). (a) the submicron particles ( $Dp < 1 \mu m$ ), and (b) the supermicron particles ( $Dp > 1 \mu m$ ), respectively.

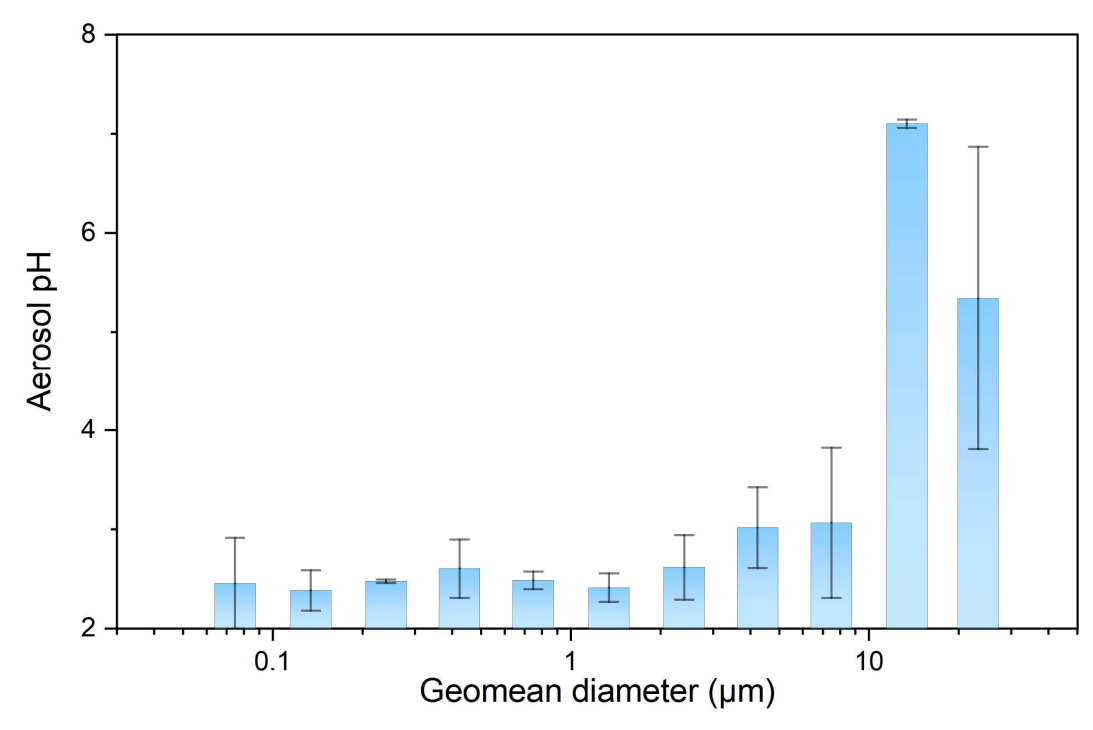


**Figure S4:** Aerosol pH simulated using ISORROPIA II model in size-resolved aerosols in the upper mixing layer of the mountain (DMS). The vertical bar represents one standard deviation.

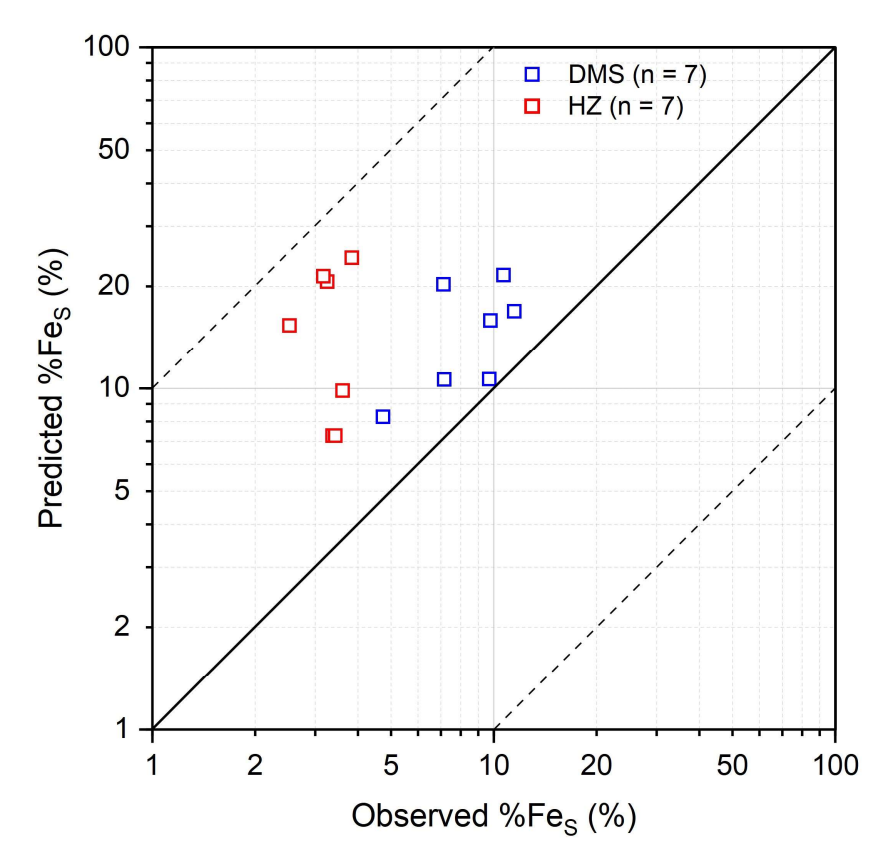


**Figure S5:** Comparison of predicted %Fes ( $D_p > 1 \mu m$ ) with field observations (TSP) over mountain (DMS) and Hangzhou (HZ). The numbers of data points were 7 and 7 in the mountain site (blue squares) and Hangzhou (red squares), respectively. The solid line represents a 1:1 reference line. The dashed lines denote deviations from the solid line by a factor of  $\pm$  10.

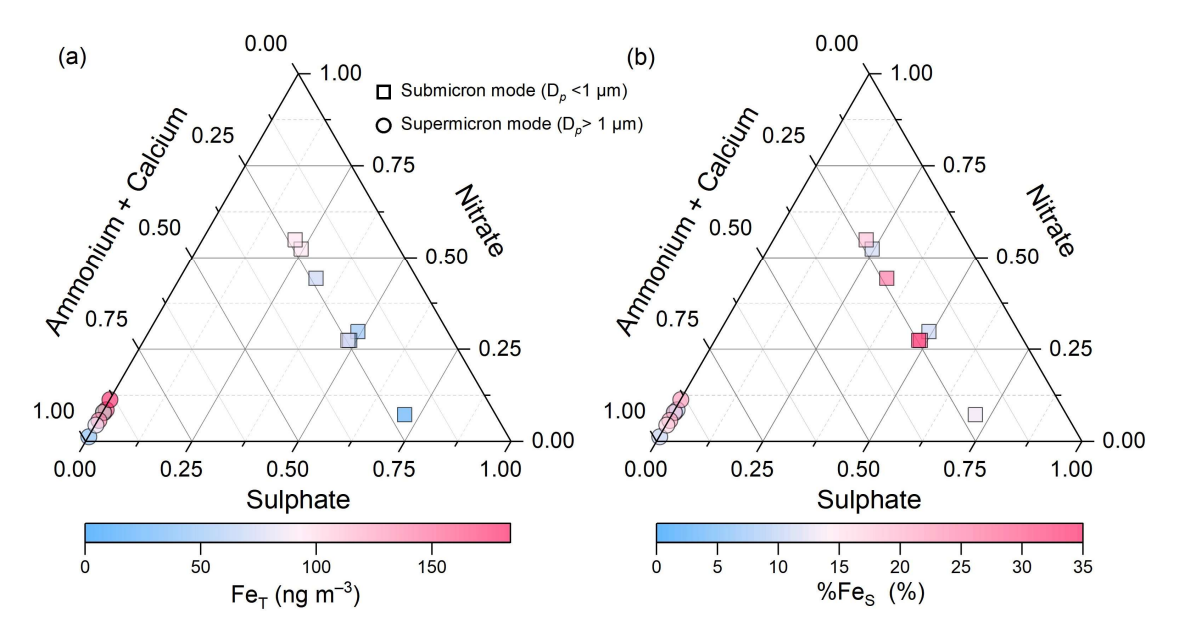


**Figure S6:** Ternary diagram of the relative abundances of sulfate, nitrate, and alkaline species (ammonium + calcium) in size-resolved aerosols simulated for Hangzhou using the Integrated Massively Parallel Atmospheric Chemical Transport (IMPACT) model. The symbols (circles and squares) are colored by total Fe (Fe<sub>T</sub>) in panel (a) and by %Fes in panel (b).

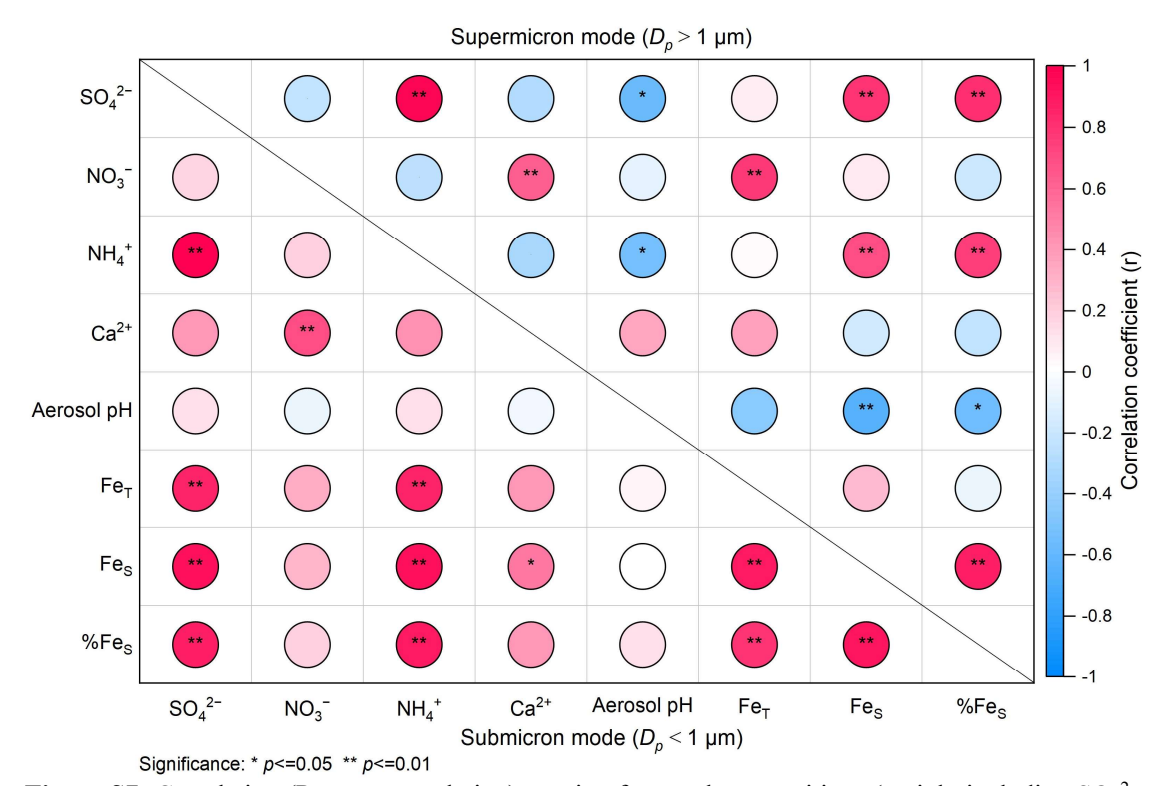


**Figure S7:** Correlation (Pearson correlation) matrix of aerosol compositions (mainly including  $SO_4^{2^-}$ ,  $NO_3^-$ ,  $NH_4^+$ , and  $Ca^{2^+}$ ), Fe<sub>T</sub>, Fe<sub>S</sub>, %Fe<sub>S</sub>, and aerosol pH in the size-resolved aerosols in DMS. The filled circles are colored by the correlation coefficients. "\*" indicates p-values less than 0.05 (p < 0.05) and "\*\*" means p-values less than 0.01 (p < 0.01).

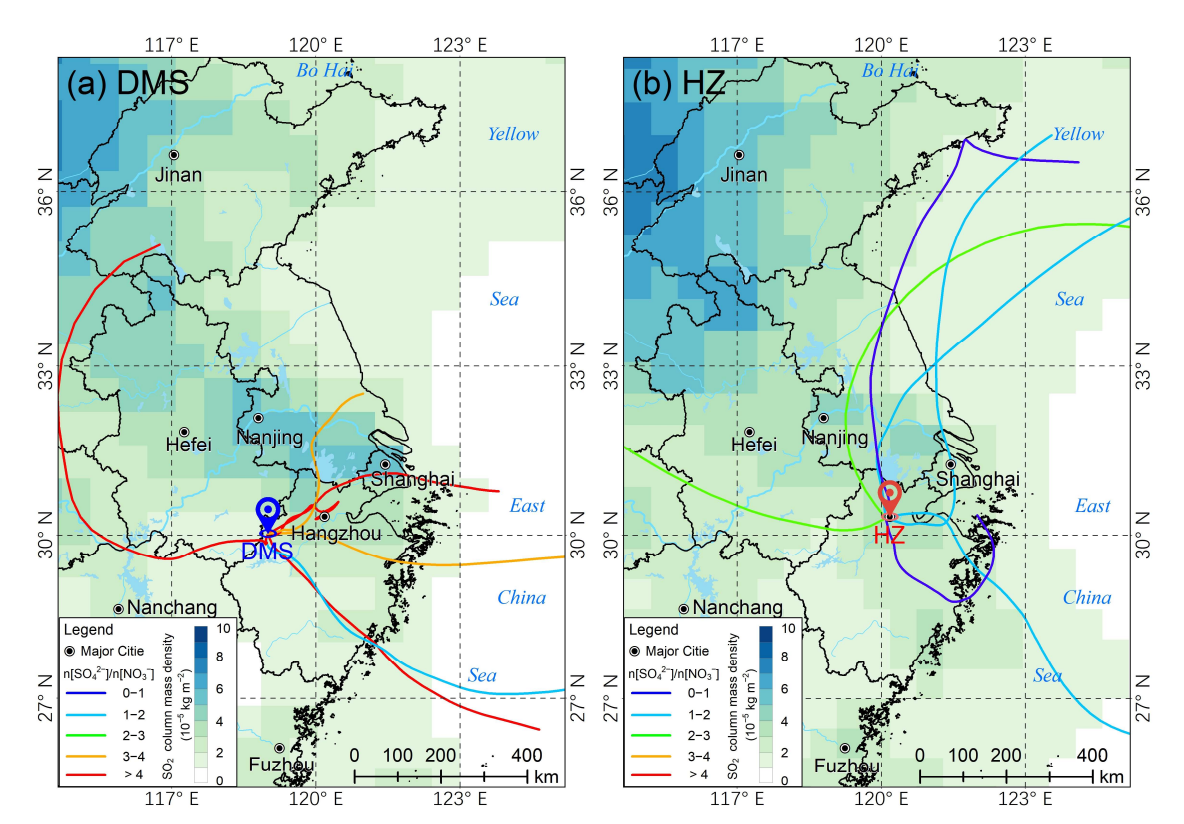


**Figure S8:** Backward air mass trajectories overlaid on SO<sub>2</sub> column mass density maps during the sampling period. (a) Mountain (DMS), and (b) Hangzhou (HZ). The color shading indicates the hourly averaged SO<sub>2</sub> column mass density (in  $10^{-5}$  kg m<sup>-2</sup>) with a spatial resolution of  $0.5^{\circ}\times0.625^{\circ}$  retrieved from Goddard Earth Sciences Data and Information Services Center (GES DISC) (available at https://giovanni.gsfc.nasa.gov/giovanni/, accessed on June 3, 2025). Colored lines represent 48-hour backward trajectories calculated using the HYSPLIT model. The line colors denote molar ratios of sulfate to nitrate ( $n[SO_4^{2-}]/n[NO_3^{-}]$  during the corresponding air mass transport periods.

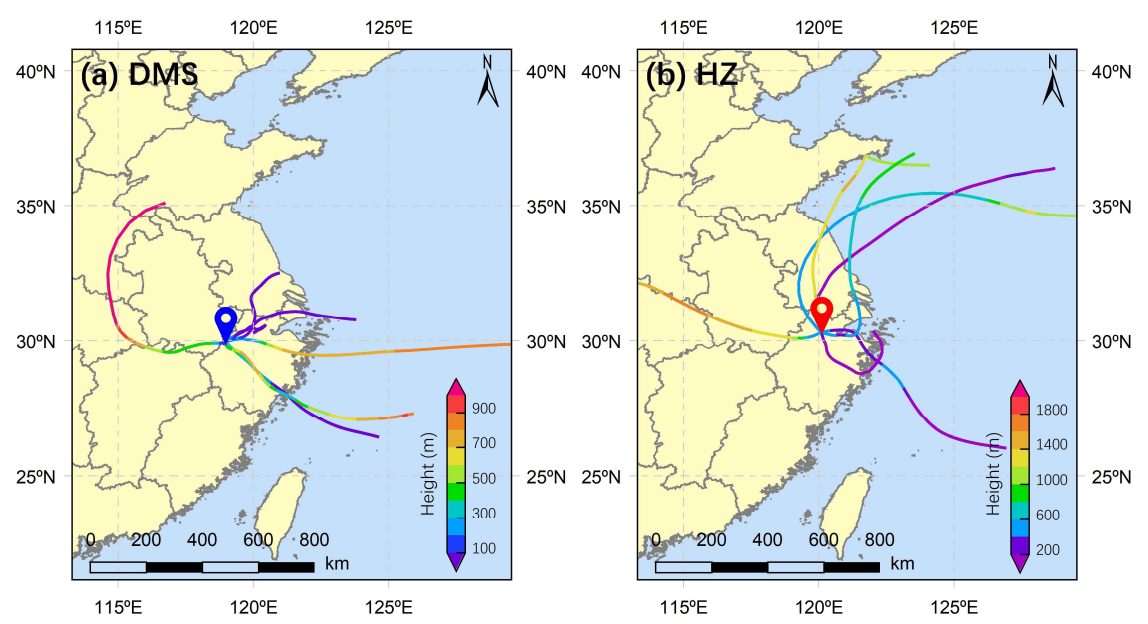


**Figure S9.** The heights (m) for 48-hr backward trajectories arriving at (a) Mountain (DMS), and (b) Hangzhou (HZ).

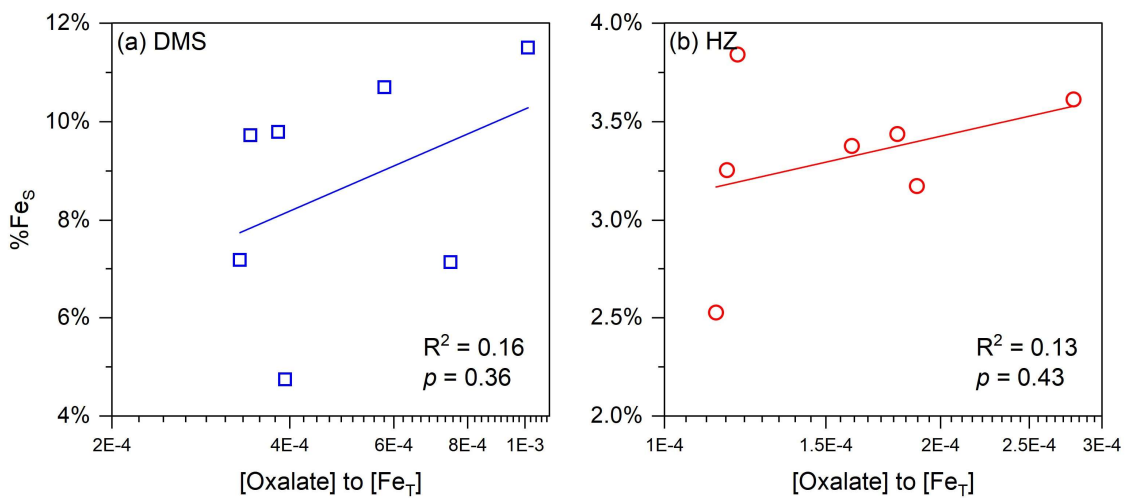


**Figure S10:** Correlations between Fe solubility and the molar ratios of oxalate to total Fe ([oxalate]/[Fe<sub>T</sub>]). (a) Mountain (DMS), and (b) Hangzhou (HZ). Linear regression is fitted in the figure.

**Table S1:** Sampling information (sampling site, number, sample time, mean temperature and relative humidity) during the field campaign.

Sampling site	NO.	Sampling time	Mean temperature (°C)	Mean relative humidity (%)
Mountain site (DMS)	M1	2021/7/17	20.88	95.63
	M2	2021/7/18-7/19*	19.40	94.68
	M3	2021/7/20-7/21*	20.49	91.47
	M4	2021/7/29-8/1*	26.90	82.97
	M5	2021/8/2	22.19	83.00
	M6	2021/8/8-8/9*	21.46	81.96
	M7	2021/8/12-8/19*	19.58	87.28
Megacity of Hangzhou (HZ)	H1	2021/9/11	27.08	82.18
	H2	2021/9/14	25.44	78.16
	H3	2021/9/16	24.76	79.48
	H4	2021/9/17	25.50	66.00
	H5	2021/9/18	25.87	61.80
	Н6	2021/9/19	27.77	67.22
	H7	2021/9/21	27.60	58.68

Note: "\*" indicates that the sampling was temporarily stopped due to rain events during the sampling period.

#### References

- Deshmukh, D. K., Kawamura, K., Kobayashi, M., and Gowda, D.: Changes in the Size Distributions of Oxalic Acid and Related Polar Compounds Over Northern Japan During Spring, J. Geophys. Res.: Atmos., 128, e2022JD038461, https://doi.org10.1029/2022jd038461, 2023.
- Fu, P. Q., Kawamura, K., Usukura, K., and Miura, K.: Dicarboxylic acids, ketocarboxylic acids and glyoxal in the marine aerosols collected during a round-the-world cruise, Mar. Chem., 148, 22–32, <a href="https://doi.org10.1016/j.marchem.2012.11.002">https://doi.org10.1016/j.marchem.2012.11.002</a>, 2013.
- Ho, K. F., Lee, S. C., Ho, S. S. H., Kawamura, K., Tachibana, E., Cheng, Y., and Zhu, T.: Dicarboxylic acids, ketocarboxylic acids, α-dicarbonyls, fatty acids, and benzoic acid in urban aerosols collected during the 2006 Campaign of Air Quality Research in Beijing (CAREBeijing-2006), J. Geophys. Res.: Atmos., 115, D19312, https://doi.org10.1029/2009jd013304, 2010.
- Ito, A. and Miyakawa, T.: Aerosol Iron from Metal Production as a Secondary Source of Bioaccessible Iron, Environ. Sci. Technol., 57, 4091–4100, <a href="https://doi.org10.1021/acs.est.2c06472">https://doi.org10.1021/acs.est.2c06472</a>, 2023.
- Ito, A. and Xu, L.: Response of acid mobilization of iron-containing mineral dust to improvement of air quality projected in the future, Atmos. Chem. Phys., 14, 3441–3459, <a href="https://doi.org10.5194/acp-14-3441-2014">https://doi.org10.5194/acp-14-3441-2014</a>, 2014.
- Ito, A., Myriokefalitakis, S., Kanakidou, M., Mahowald, N. M., Scanza, R. A., Hamilton, D. S., Baker, A. R., Jickells, T., Sarin, M., Bikkina, S., Gao, Y., Shelley, R. U., Buck, C. S., Landing, W. M., Bowie, A. R., Perron, M. M. G., Guieu, C., Meskhidze, N., Johnson, M. S., Feng, Y., Kok, J. F., Nenes, A., and A., D. R.: Pyrogenic iron: The missing link to high iron solubility in aerosols, Sci. Adv., 5, eaau7671, https://doi.org10.1126/sciadv.aau7671, 2019.
- Li, W. J., Ito, A., Wang, G. C., Zhi, M. K., Xu, L., Yuan, Q., Zhang, J., Liu, L., Wu, F., Laskin, A., Zhang, D. Z., Zhang, X. Y., Zhu, T., Chen, J. M., Mihalopoulos, N., Bougiatioti, A., Kanakidou, M., Wang, G. H., Hu, H. L., Zhao, Y., and Shi, Z. B.: Aqueous-phase secondary organic aerosol formation on mineral dust, Natl. Sci. Rev., nwaf221, <a href="https://doi.org10.1093/nsr/nwaf221/8154540">https://doi.org10.1093/nsr/nwaf221/8154540</a>, 2025.
- Sakata, K., Kurisu, M., Takeichi, Y., Sakaguchi, A., Tanimoto, H., Tamenori, Y., Matsuki, A., and Takahashi, Y.: Iron (Fe) speciation in size-fractionated aerosol particles in the Pacific Ocean: The role of organic complexation of Fe with humic-like substances in controlling Fe solubility, Atmos. Chem. Phys., 22, 9461–9482, https://doi.org10.5194/acp-22-9461-2022, 2022.
- Shi, J., Guan, Y., Gao, H., Yao, X., Wang, R., and Zhang, D.: Aerosol Iron Solubility Specification in the Global Marine Atmosphere with Machine Learning, Environ. Sci. Technol., 56, 16453–16461, <a href="https://doi.org10.1021/acs.est.2c05266">https://doi.org10.1021/acs.est.2c05266</a>, 2022.
- Yang, J. and Huang, X.: The 30 m annual land cover dataset and its dynamics in China from 1990 to 2019, Earth Syst. Sci. Data, 13, 3907–3925, <a href="https://doi.org10.5194/essd-13-3907-2021">https://doi.org10.5194/essd-13-3907-2021</a>, 2021.

- Yu, J. Z., Huang, X. F., Xu, J., and Hu, M.: When Aerosol Sulfate Goes Up, So Does Oxalate-Implication for the Formation Mechanisms of Oxalate, Environ. Sci. Technol., 39, 128–133, <a href="https://doi.org10.1021/es049559f">https://doi.org10.1021/es049559f</a>, 2005.
- Zhang, H., Li, R., Dong, S., Wang, F., Zhu, Y., Meng, H., Huang, C., Ren, Y., Wang, X., Hu, X., Li, T., Peng, C., Zhang, G., Xue, L., Wang, X., and Tang, M.: Abundance and Fractional Solubility of Aerosol Iron During Winter at a Coastal City in Northern China: Similarities and Contrasts Between Fine and Coarse Particles, J. Geophys. Res.: Atmos., 127, e2021JD036070, <a href="https://doi.org10.1029/2021jd036070">https://doi.org10.1029/2021jd036070</a>, 2022.